DOI: 10.1002/chem.200500905

Studies on Cage-Type Tetranuclear Metal Clusters with Ferrocenylphosphonate Ligands

Jie Wu,[a] Yinglin Song,[b] Erpeng Zhang,[a] Hongwei Hou,*[a] Yaoting Fan,[a] and Yu Zhu[a]

Abstract: Reaction of $FcCH_2PO_3H_2$ [$Fc=(\eta^5\text{-}C_5H_5)Fe(\eta^5\text{-}C_5H_4)$] ($H_2FMPA$) and 1,10-phenanthroline (phen) with $Cd(OAc)_2\cdot 2H_2O$ or $ZnSO_4\cdot 7H_2O$ in methanol in the presence of triethylamine resulted in the formation of two new ferrocenylphosphonate metal-cage complexes $[M_4(fmpa)_4(phen)_4]\cdot 7CH_3OH$ (M = Cd **1**, M = Zn **2**). Both structures contain two kinds of isomeric tetranuclear metal phosphonate cages, which are linked to one another by π–π interactions between the phen molecules. In **1**, the Cd1, Cd3, and Cd4 atoms are all pentacoordinate, while the Cd2 atom is coordinated by four oxygen atoms from three phosphonate ligands and two nitrogen atoms from the chelating phen in a distorted octahedral geometry. Four Cd atoms from each unit are interconnected through bridging phosphonate ligands with different coordination modes, such as 5.221, 4.211, and 2.11 (Harris notation), yielding a $\{Cd_4\}$ cage. In **2**, each Zn atom is coordinated by three oxygen atoms from three phosphonate ligands and two nitrogen atoms from phen, leading to a distorted square-pyramidal geometry. The four Zn atoms of each isomeric unit are also interconnected through four bridging phosphonate ligands to yield a $\{Zn_4\}$ cage. Fluorescent studies indicate that ligand-to-ligand charge-transfer photoluminescence is observed for **1**, while the emisson bands of **2** can be assigned to an admixture of ligand-to-ligand and metal-to-ligand charge transfer. Solution-state differential pulse voltammetry indicates that the half-wave potentials of the ferrocenyl moieties in **1** and **2** have different deviations relative to the relevant H_2FMPA ligand. This may be because the highest occupied molecular orbital (HOMO) in **1** is located in the $FMPA^{2-}$ groups, while in **2** the HOMO is located in the phen and Zn^{II} groups, so the Fe^{II} centers in complex **1** are more easily oxidized to Fe^{III} centers than those of **2**. The third-order nonlinear optical (NLO) measurements show that both **1** and **2** exhibit strong third-order NLO self-focusing effects; hence, they are promising candidates for NLO materials. By calculating the component of the lowest unoccupied molecular orbitals of **1** and **2**, we confirmed that the co-planar phen rings control their optical nonlinearity, while the H_2FMPA ligands and metal ions have only a weak influence on their NLO properties.

Keywords: cluster compounds · density functional calculations · ferrocene · nonlinear optics · phosphonate ligands

Introduction

Metal phosphonates have attracted a substantial amount of research interest due to their potential applications in many areas such as ion exchange, catalysis, sensors, proton conductivity, nonlinear optics, and materials chemistry,[1–6] many of which can be attributed to the extensive structural and compositional diversity of these systems. Metal phosphonates usually exhibit 1D chain, 2D layer, and 3D network with micropore structures, of which the 2D layer structure is the most common.[1–6] However, cage complexes featuring phosphonate ligands are relatively rare. This may be due to the fact that metal phosphonates have very poor solubility, so that they are frequently found in polymeric coordination complexes rather than in cage complexes.[7] Several metal phosphonate clusters have been described in recent years, including iron,[7] zinc,[8–12] cadmium,[13] copper,[14,15] cobalt,[16,17] manganese,[18,19] gallium,[20] tin,[21] and vanadium[22] cages, all of which exhibit intriguing structures and properties. For example, Chandrasekhar and Kingsley re-

[a] J. Wu, E. Zhang, Prof. H. Hou, Prof. Y. Fan, Y. Zhu
Department of Chemistry, Zhengzhou University
Zhengzhou, 450052 (China)
Fax: (+86) 371-6776-1744
E-mail: houhongw@zzu.edu.cn

[b] Prof. Y. Song
Department of Applied Physics
Harbin Institute of Technology, Harbin, 150006 (China)

Supporting information for this article is available on the WWW under http://www.chemeurj.org/ or from the author.

ported a novel $\{Cu_{12}\}$ cage with antiferromagnetically coupled behavior,[14] the Winpenny group synthesized $\{Co_{13}\}$ and $\{Mn_6\}$ cages with interesting magnetic properties,[16] and redox-active $\{Mn_4\}$ cages have been described by the Dismukes group.[18] All these results led us to pay more attention to phosphonate cage complexes.

Besides their various structures, another interesting feature of metal phosphonates is the diverse range of functional groups that can be introduced to the phosphonic acid precursors, thus allowing the design of materials with specific properties. Most studies to date have been carried out on phenylphosphonic and alkylphosphonic acids.[23–25] Phosphonic acids with other organic functional groups such as azacrown ethers,[26–28] amines,[29–31] sulfonate/sulfonic acid[32,33] and carboxylate/carboxylic acid groups[34–37] have been found to be better ligands that can form many complexes with novel structures and properties. Motivated by the current work on functional coordinate materials bearing ferrocene (Fc) groups, we have synthesized a ferrocenylphosphonic acid, and subsequently used it for coordination with metal salts, thus yielding materials displaying both ferrocene and metal–phosphonate properties in conjunction with robust inorganic backbones.

Although several ferrocenylphosphonic acids have previously been prepared, their metal complexes are extremely rare.[38,39] This is because metal phosphonates normally form poorly crystalline compounds and the ferrocene moiety is sensitive to oxygen, water, heat, and light when it is attached with electron-withdrawing substituents on the cyclopentadienyl (Cp) rings.[40–42] Until now, only Henderson et al. have reported platinum–ferrocenylphosphonate complexes and studied their antitumor activity[39] and Bideau et al. have reported a zinc(II)–ferrocenylphosphonate polymer with a unique 2D ferrocene arrangement anchored on a 1D Zn-O-P-O-Zn backbone.[38] To the best of our knowledge, metal–ferrocenylphosphonate cage complexes have not been reported. To achieve the synthesis of such complexes we decided to utilize an ancillary ligand such as 1,10-phenanthroline (phen), the chelating effect of which usually results in metal phosphonates with a lower dimensionality.[35] Herein we report on the synthesis and crystal structures of two novel metal–ferrocenylphosphonate cage complexes, $[M_4(fmpa)_4(phen)_4]\cdot 7CH_3OH$ (M = Cd **1**, Zn **2**; $H_2FMPA = FcCH_2PO_3H_2$). Both structures are found to have twin molecular systems and tetranuclear metal cores bound to the H_2FMPA and phen ligands. The electrochemical, fluorescent, and NLO properties of these complexes have been investigated. In addition, by using quantum chemistry calculations we have proposed the possible fluorescent emission mechanisms for **1** and **2**, and confirmed the effect of the metal ions and organic ligands on their NLO properties.

Results and Discussion

Synthesis: Metal phosphonates are usually prepared by reaction of a metal salt with a phosphonic acid by a hydrothermal method, coprecipitation in solution, or a melt method; the hydrothermal method is regarded as the most effective. It is often the case, however, that the metal phosphonate is formed too rapidly to allow growth of crystals sufficiently large to be suitable for structural determination.[43] Most structurally characterized phosphonates are found in polymeric coordination complexes.

The use of the additional bidentate metal linker, phen, has been successful in yielding metal complexes with a low dimensionality, for example, molecular clusters, because of its chelating effect.[35] Therefore, to synthesize metal ferrocenylphosphonate complexes with a cage framework, we treated phen with $Cd(OAc)_2\cdot 2H_2O$ or $ZnSO_4\cdot 7H_2O$ at room temperature, then an admixture of H_2FMPA and triethylamine was added dropwise , and intensely colored solutions were produced. The resulting orange solutions were allowed to stand at room temperature in the dark. After one week, yellow single crystals suitable for X-ray diffraction studies were obtained. These crystals are unstable, slowly losing their shape in the air. Both complexes are insoluble in common organic solvents, such as MeOH, EtOH, MeCN, and THF, but are slightly soluble in highly polar solvents such as dimethylsulfoxide (DMSO) or DMF.

X-ray crystal structure of $[Cd_4(fmpa)_4(phen)_4]\cdot 7CH_3OH$ (1): Single-crystal structural determinations reveal that **1** crystallizes in the space group $P\bar{1}$; the structure consists of two isomeric units, each unit comprising four Cd atoms interconnected through four bridging phosphonate ligands to yield a cage. As shown in Figure 1, each symmetry unit is composed of four FMPA groups, four phen groups, and four Cd atoms. The differences between the two crystallographic isomers are that the $FMPA^{2-}$ groups have different orientations and the Cd atoms adopt different types of coordination geometries. The first unit (Figure 1, left) contains two kinds of crystallographically independent Cd atoms with different types of coordination geometries. The Cd1 atom is coordinated by two N atoms (N1, N2) from the chelating phen and three O atoms (O2A, O3, O6) from three phosphonate ligands. The Cd2 atom exhibits a distorted octahedral geometry with four O atoms (O1A, O2, O3, O4A) from three phosphonate ligands and two N atoms (N3, N4) from the chelating phen. The four Cd centers (Cd1, Cd1A, Cd2, and Cd2A) form a rectangle, and are held in place by four FMPA groups, forming the cage structure (Figure 2). The Cd1···Cd2 and Cd1···Cd2A distances are 3.871 and 3.591 Å, respectively, and the angles of Cd2···Cd1···Cd2A and Cd1···Cd2···Cd1A are 88.0 and 92.0°, respectively. We note that the H_2FMPA ligands exhibit two types of coordination modes with different conformations in this isomeric unit. One phosphonate ligand (P1) bridges five Cd atoms through a monodentate coordinated O atom (O1) and two μ_2-bridging coordinated O atoms (O2, O3), which can be described by using Harris notation[44] as a 5.221 mode (see Scheme 1), while the P2 ligand adopts a 2.11 mode.

The second isomer, unit two, (Figure 1, right) has a similar cadmium cage to that mentioned above, with the four Cd

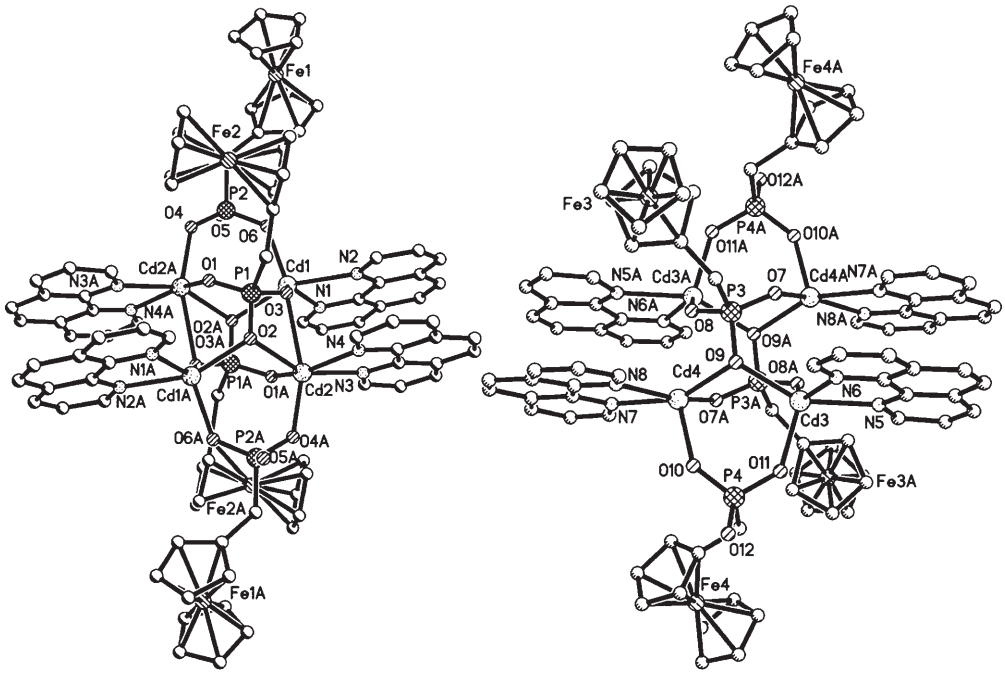

Figure 1. ORTEP representation of unit one (left) and unit two (right) of **1**. Hydrogen atoms and solvent molecules have been omitted for clarity.

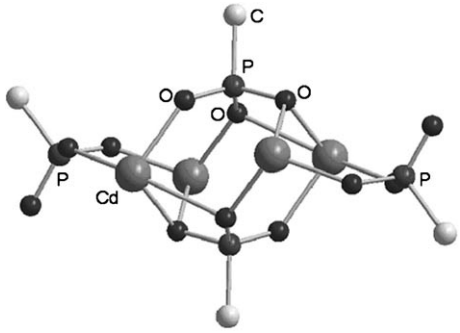

Figure 2. DIAMOND view of a unit of **1**, emphasizing the cage feature. Ferrocene, phen, and solvent molecules have been omitted for clarity.

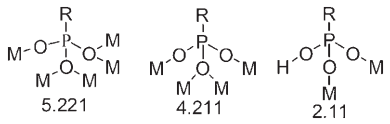

Scheme 1. The bonding modes displayed by the phosphonate ligand, with the Harris notation for each mode.

atoms all pentacoordinate. The P4 ligand adopts a 2.11 mode, similar to P2. The P3 ligand has one μ_2-bridging coordinated O atom (O9) and two monodentate coordinated O atoms (O7, O8); using Harris notation[44] this can be described as a 4.211 mode. So in complex **1**, the H_2FMPA ligand adopts three different coordination modes (5.221, 4.211, and 2.11), which is unusual in metal phosphonates. The Cd–O distances range from 2.138(5) to 2.642(5) Å, with an average of 2.258 Å, close to that of the reported leaflet structure $[Cd_4(LH{\cdot}H_2O)_3(H_2O)_5(NO_3)_4][NO_3]$ (H_2L = *N*-(phosphonomethyl)aza[18]crown-6).[26] The distance between the bridging oxygen atom O3 and Cd2 is 2.642(5) Å, which is the longest of all the Cd–O and Cd–N distances.

The coplanar phen rings with deviations in the range of 0.020–0.036 Å are parallel to each other, and the dihedral angles between adjacent phen planes range from 3.4–4.9° (Figure 3). The average interplanar distance of these parallel phen ligands is 3.543 Å, which is within the common range for π–π interactions between two aryl rings. Tetrametallic units are linked by these π–π interactions, which are important in the molecular assembly.

X-ray crystal structure of $[Zn_4(fmpa)_4(phen)_4]{\cdot}7CH_3OH$ (2): The crystal structure of **2,** like complex **1,** displays two isomeric centrosymmetric tetrameric building units. However, the Zn atoms adopt different coordination modes from the Cd atoms in **1**. All the Zn atoms are coordinated by five donors in a distorted square-pyramidal geometry. The donors include three O atoms from three H_2FMPA ligands and two N atoms from the chelating phen (Figure 4). The four Zn atoms of each isomeric unit also form a rectangle and are interconnected through four bridging phosphonate ligands to yield a cage. The Zn···Zn distances are in the range of 3.438–3.870 Å. The angles of Zn2···Zn1···Zn2A, Zn1···Zn2···Zn1A, Zn4···Zn3···Zn4A and Zn3···Zn4···Zn3A are 88.2, 91.8, 87.6, and 92.4°, respectively. The other main difference between **1** and **2** is that the H_2FMPA ligands of **2** adopt only two kinds of coordination modes. One kind of phosphonate ligand, P2 (or P3), adopts a 2.11 mode, while the other kind, P1 (or P4), adopts a 4.211 mode. The O1 atom forms a bridge between a pair of metal atoms, and the O2 (or O3) atom is coordinated to just one metal atom. The

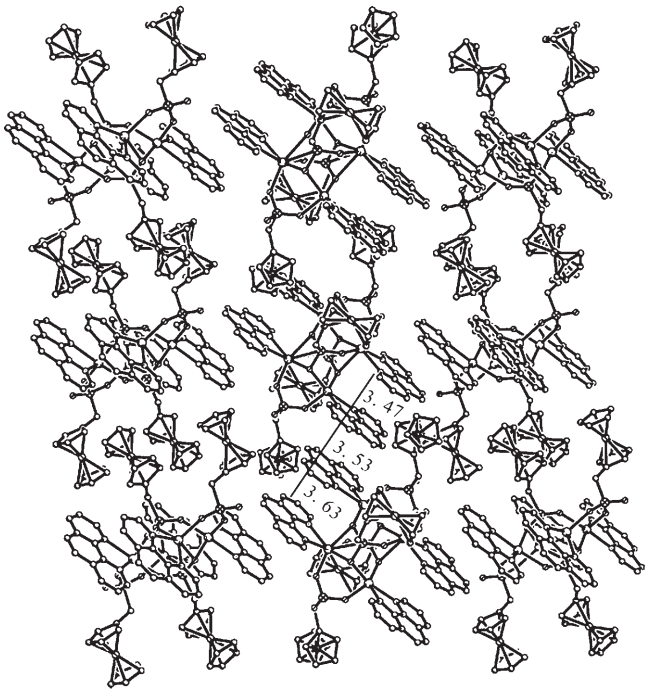

Figure 3. Crystal packing view of the structure of **1** along the *b* axis. Hydrogen atoms and solvent molecules of crystallization are omitted for clarity.

Photoluminescent properties: The photoluminescent properties of phen, H_2FMPA, and complexes **1** and **2** were investigated in the solid state at room temperature. Excitation at 241 nm leads to broad violet fluorescence signals with the emission maxima at approximately 382 nm for phen, 388 nm for H_2FMPA, 386 nm for **1**, and 391 nm for **2** (Figure 5). To better understand the observed luminescent properties, molecular orbital (MO) calculations[45–46] were applied to complexes **1** and **2**. Figure 6 depicts the frontier molecular orbitals of **1**. The highest occupied molecular orbital (HOMO) of **1** is located in the $FMPA^{2-}$ groups, while the lowest unoccupied molecular orbital (LUMO) is on the π*-antibonding orbitals from the phen ligands and some oxygen atoms of the phosphonate ligands. Therefore, we suggest that the emission bands can be assigned to the ligand-to-ligand charge-transfer (LLCT) emission. In **2**, the HOMO is mainly associated with the phen ligands and 3d orbitals of Zn^{II}, while the LUMO is composed mainly of the π*-antibonding orbitals from the phen and also of the Zn^{II} unoccupied orbital based on 4s, thus its photoluminescent property can be assigned to metal-to-ligand charge transfer (MLCT), admixed with the LLCT, which originates from the adjacent phen ligands (Figure 7). The different charge-transfer mechanisms of **1** and **2** can be attributed to the fact that the Zn^{II} ions in the rigid cages of **2** have more powerful electron-withdrawing effects than the Cd^{II} ions in complex **1**.

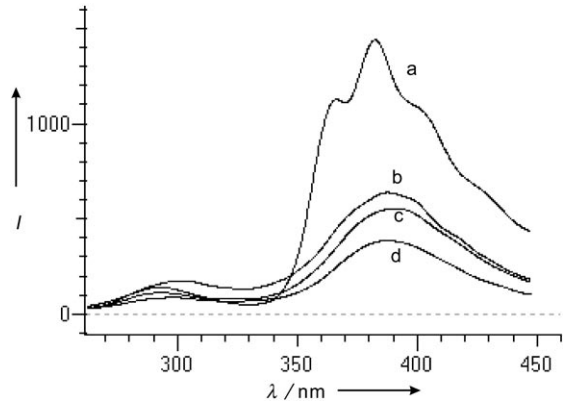

Figure 5. Fluorescent emission spectra of a) phen, b) H_2FMPA, c) **2** and d) **1** in the solid state upon excitation at 241 nm at room temperature.

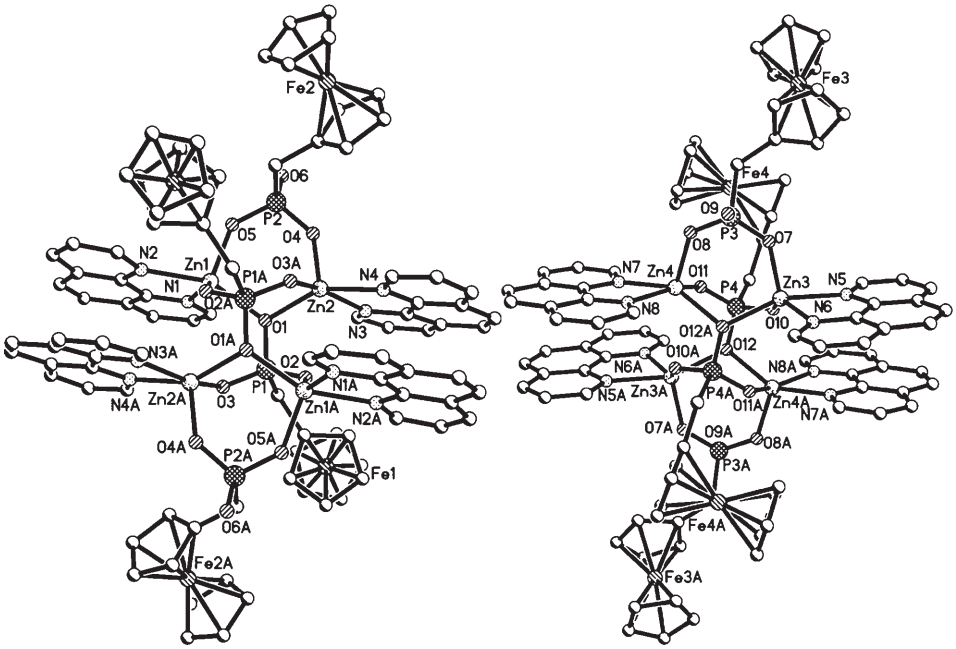

Figure 4. ORTEP representation of unit one (left) and unit two (right) of **2**. Hydrogen atoms and solvent molecules have been omitted for clarity.

Zn−O distances range from 1.915(5) to 2.165(5) Å and the Zn−N distances range from 2.122(7) to 2.222(6) Å, similar to other zinc(II) phosphonates.[29,38] The P−O distances, although slightly different from each other, have an average value of 1.523 Å, which is similar to that found for complex **1** (1.521 Å).

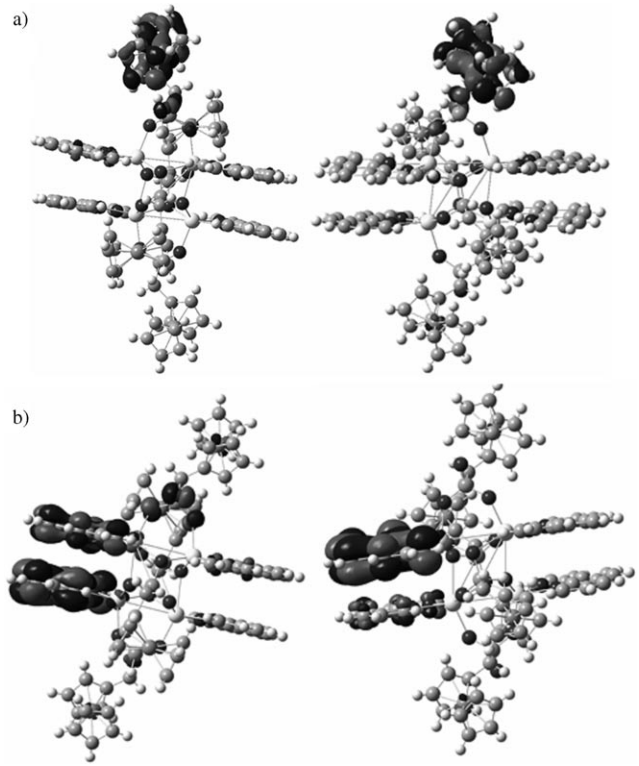

Figure 6. The frontier molecular orbital of **1:** a) HOMO; b) LUMO.

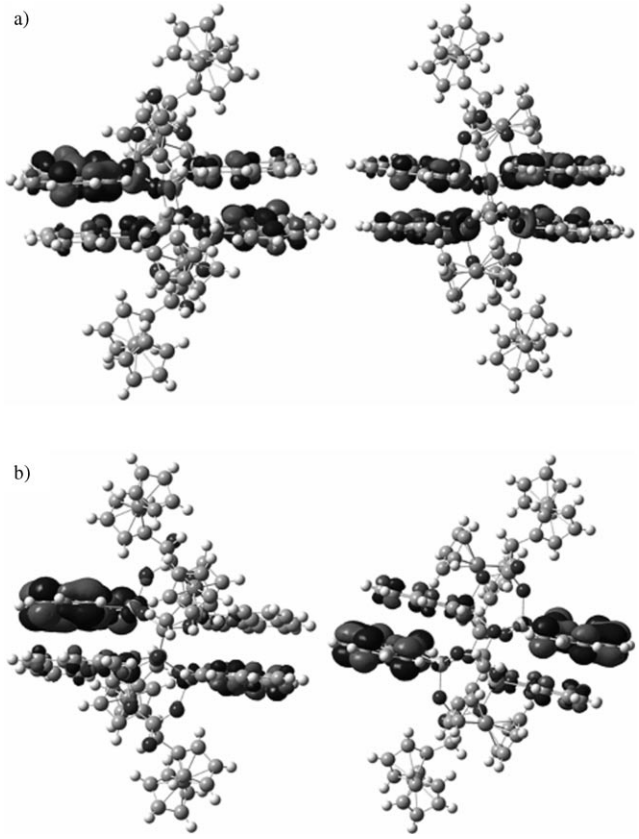

Figure 7. The frontier molecular orbital of **2:** a) HOMO; b) LUMO.

Electrochemistry: The solution-state differential pulse voltammetry for **1**, **2**, and H_2FMPA shows single peaks with half-wave potentials at 0.352, 0.436, and 0.372 V (vs. SCE), respectively (Figure 8). These observed redox peaks are due

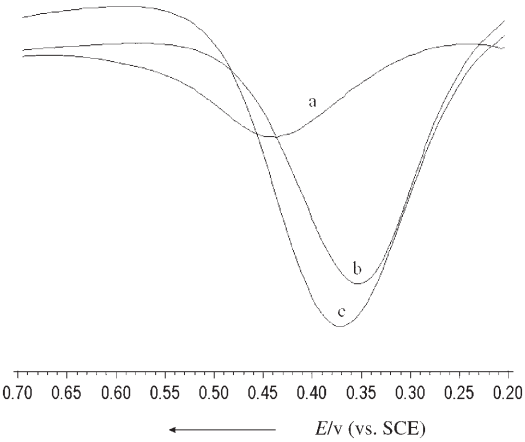

Figure 8. Differential pulse voltammogram of a) **2**, b) **1**, and c) H_2FMPA (1.0×10^{-3} M) in DMF containing nBu$_4$NClO$_4$ (0.1 M) at a scan rate of 20 mV s^{-1} (vs. SCE).

to the single-electron Fe^{II}/Fe^{III} couple oxidation process. The redox peak of **1** shifts to a slightly lower potential relative to H_2FMPA, while that of **2** shifts to a higher potential. The different deviations in the electrochemical behavior of **1** and **2** relative to that of H_2FMPA may be due to the following effects. According to our previous reports, the metal ions in complexes have a significant influence on the half-wave potentials of the ferrocenyl moieties, due to the different electron-withdrawing natures of the coordinated metal centers,[49] and can cause the Fe^{II}/Fe^{III} oxidation potential of ferrocene-containing complexes to shift to a higher or lower potential in comparison with their corresponding ligands.[47–48] Frontier orbital theory may provide an explanation for such behavior.[50] In **2**, the HOMO is associated with the phen ligands and Zn^{II} orbitals, and the charge transitions of the tetranuclear metal cores may play an important role in the change of the Fe^{II}/Fe^{III} oxidation potential. The HOMO in **1** is located in the FMPA^{2-} groups, so the Fe^{II} centers of **1** are more easily oxidized to Fe^{III} than those in complex **2**.

NLO properties: Compared with traditional inorganic NLO materials, coordination compounds have many advantages:[51]

1) Ligands present high electronic susceptibility ($\chi^{(3)}$) through high molecular hyperpolarizability[52,53] and their structures can be tailored in numerous ways to tune NLO properties for desired applications, by introducing different organic groups into the ligands.
2) The metal center may be an extremely strong donor or acceptor, since it may be electron rich or poor depending on its oxidation state and ligand environment.[52]

The third-order nonlinear activities of the coordination compounds are evidently affected by incorporation of the central metal atom, by the introduction of intense metal→ligand and ligand→metal charge transfer.[54,55] It has been reported that the strength of NLO properties can be boosted by the π-back-donation capacity of metal ions to ligands.[56]

The UV/Vis absorption spectra of H_2FMPA and complexes **1** and **2** were determined in DMF (Figure 9). All these compounds have relatively low linear absorption ranging from 500–800 nm, promising low-intensity loss and little temperature change caused by photon absorption when light propagates in the materials. In addition, UV/Vis absorption spectra demonstrate that the NLO responses are clear without interference of other absorption at $\lambda = 532$ nm used in the *Z*-scan technique.

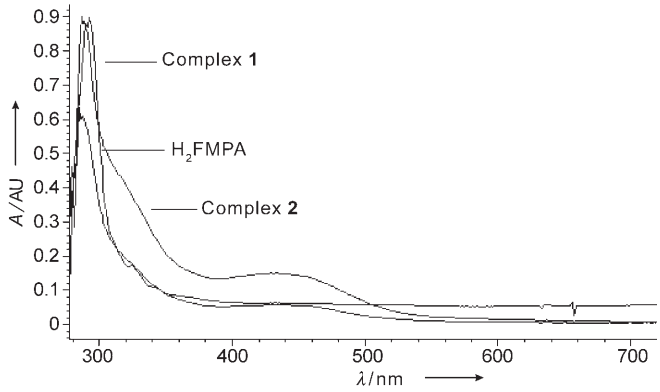

Figure 9. The UV/Vis spectra of **1**, **2** and H_2FMPA in DMF.

The third-order NLO properties of **1**, **2** and H_2FMPA were investigated with 532 nm laser pulses of 8 ns duration by a *Z*-scan experiment in DMF with concentrations of 1.99×10^{-4}, 2.16×10^{-4}, and 2.24×10^{-4} mol dm^{-3}, respectively. The nonlinear refractive components were assessed by dividing the normalized *Z*-scan data obtained under the closed aperture configuration by that obtained under the open aperture configuration. The experimental results show that H_2FMPA exhibits very weak NLO behavior, but complexes **1** and **2** show evident third-order NLO self-focusing behavior, plotted in Figures 10a and 10b, respectively. The filled squares are the experimental data and the solid curves are the theoretical fit by using Z-scan theory,[57] and it is clear that the theoretical curve qualitatively reproduces the experimental data well. The reasonably good fit between the experimental and theoretical curves suggests that the experimentally obtained NLO effects are third-order in nature. The data reveals that complexes **1** and **2** both have a positive sign for the refractive nonlinearity, and the valley/peak pattern of the normalized transmittance curve shows characteristic self-focusing behavior. From the theoretical curves, the third-order NLO effective index n_2 is 4.08×10^{-11} esu for **1** and 4.24×10^{-11} esu for **2**. The effective third-order nonlinear optical susceptibilities $\chi^{(3)}$ of these complexes were determined by comparing the signal intensities with that of CS_2, by subtracting the relatively weak background noise and the contribution of the solvent. The $\chi^{(3)}$ value of CS_2 was taken as 6.2×10^{-13} esu under the same experimental conditions, consistent with the literature.[58] The effective third-order NLO susceptibilities $\chi^{(3)}$ obtained are 2.80×10^{-11} esu for **1** and 2.91×10^{-11} esu for **2**; the corresponding hyperpolarizability γ values are 7.77×10^{-29} esu for **1** and 7.47×10^{-29} esu for **2**.

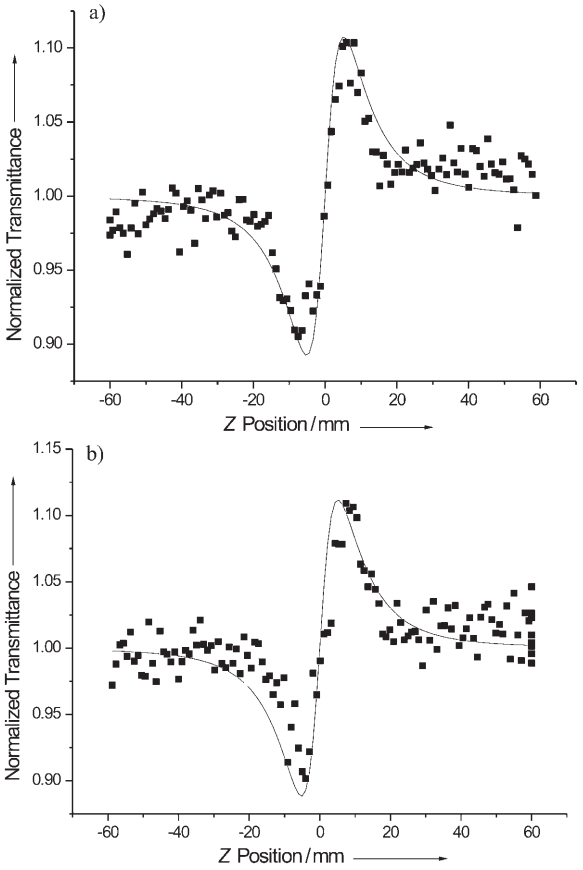

Figure 10. NLO refractive properties: a) **1** in DMF (concentration: 1.6×10^{-4} mol dm^{-3}), b) **2** in DMF (concentration: 1.7×10^{-4} mol dm^{-3}). The black squares ■ are the experimental data, and the solid curve is the theoretical fit.

To the best of our knowledge, all research confirms that the incorporation of heavy metal ions in coordination compounds has a very important effect on the third-order NLO properties, as this introduces more sublevels into the energy hierarchy, thus permitting more allowed electronic transitions and giving larger NLO effects.[59,60] However, our recent research shows that we can estimate the contribution of metal ions and ligands to the NLO properties by calculating the component of the frontier molecular orbital, and deducing whether the metal ions or ligands play the more important role in determining the NLO properties.[61] Moreover, the photochemical and photophysical properties of compounds are governed by the first excited singlet state S_1 and the first excited triplet state T_1.[62] The electron in the

HOMO is excited to the LUMO, resulting in the state S_1 or T_1; we therefore regard the LUMO as the most important frontier orbital influencing the NLO properties.

It can be seen from Figure 6 that the LUMOs of **1** are governed by the phen (with DFT/B3LYP 89.37 and 98.2% for units one and two, respectively) and some oxygen atoms of phosphonate ligands (with DFT/B3LYP 5.54% for unit one); this orbital barely has any Cd^{II} character (with DFT/B3LYP 1.1 and 0.74% for $(Cd^{II})_4$ for units one and two, respectively). So we deduce that the NLO properties of **1** are controlled by phen and influenced slightly by the oxygen atoms from the phosphonate ligands, with the Cd^{II} ions having no influence on the NLO properties. Figure 7 shows that the LUMO of **2** is primarily phen (with DFT/B3LYP 85.4 and 97.56% for units one and two, respectively) and Zn^{II} (with DFT/B3LYP 11.28 and 2.04% for $(Zn^{II})_4$ of units one and two, respectively) character. So in **2**, the NLO properties are dominated by phen, but are also affected by Zn^{II} ions. It can be seen from the results that the coplanar phen rings control the optical nonlinearity of **1** and **2**, while the H_2FMPA ligands and metal ions have a weak influence on their NLO properties. This is consistent with the experimental results: both **1** and **2** show the same NLO refractive behavior (self-focusing effect), and have a similar refractive index n_2; however, H_2FMPA exhibits very weak NLO behavior.

Conclusion

Ancillary chelating ligands usually result in metal complexes with a lower dimensionality, meaning we could obtain novel metal–ferrocenylphosphonate cage complexes with additional phen ligands. By calculating the component of the frontier molecular orbital, we proposed the possible fluorescent emission mechanisms for **1** and **2**, and studied their electrochemical behavior. In addition, we deduced the contribution of metal ions and ligands to the NLO properties by analyzing the component of the lowest unoccupied molecular orbital (LUMO). The consistency of our experimental results with inferences from quantum chemistry calculations further confirmed that the origin of the NLO properties is the delocalization of the π-electron cloud, and that it is reasonable to investigate the NLO properties of metal complexes by using frontier molecular orbital theory. Based on molecular orbital (MO) calculations we can obtain materials with better photochemical and photophysical properties accurately and easily, and studies are in progress to design particular ferrocenylphosphonate complexes with preeminent chemical and physical properties.

Experimental Section

Materials and physical techniques: All chemicals were of reagent grade quality, obtained from commercial sources, and used without further purification. H_2FMPA was prepared by literature methods.[63] IR data were recorded on a Nicolet NEXUS 470-FTIR spectrophotometer with KBr pellets in the 400–4000 cm^{-1} region. UV/Vis spectra were obtained on an HP 8453 spectrophotometer. Elemental analyses (C, H, and N) were carried out on a Carlo-Erba1106 elemental analyzer.

Preparation of complexes 1 and 2: Both complexes were synthesized by a similar method. Phen (19.8 mg; 0.1 mmol) in MeOH (4 mL) was added to a solution of $Cd(OAc)_2{\cdot}2H_2O$ (21.4 mg, 0.1 mmol) or $ZnSO_4{\cdot}7H_2O$ (28.7 mg, 0.1 mmol) in methanol (2 mL). H_2FMPA (28.0 mg; 0.1 mmol) and triethylamine (40.4 mg; 0.2 mmol) in MeOH (4 mL) were added dropwise to the mixture at room temperature and stirred overnight. The precipitate was filtered and the resulting orange solution was allowed to stand at room temperature in the dark. After one week good quality yellow crystals were obtained.

Data for ***1***: Yield: 14%; elemental analysis calcd (%) for for $C_{99}H_{104}Cd_4Fe_4N_8O_{19}P_4$: C 47.39, H 4.15, N 4.47; found: C 48.35, H 4.09, N 4.61; IR (KBr): $\tilde{\nu}$ = 3442 (s), 1627 (m), 1585 (w), 1426 (m), 1110 (m), 852 (m), 726 (m), 487 cm^{-1} (m).*Data for* ***2***: Yield: 12%; elemental analysis calcd (%) for$C_{99}H_{104}Fe_4N_8O_{19}Zn_4$: C 51.24, H 4.49, N 4.83; found: C 50.74, H 4.52, N 4.88; IR (KBr): $\tilde{\nu}$ = 3423 (s), 1625 (m), 1516 (w), 1426 (m), 1102 (m), 848 (m), 728 (m), 487 cm^{-1} (m).

Luminescent measurements: The luminescent spectra were measured on powder samples at room temperature by using a model F-4500 Hitachi Fluorescence Spectrophotometer. The excitation and emission slits were both 5 nm, and the response time was 2 s.

Computational methods: On the basis of crystal structures, B3LYP[64–66] calculations were carried out for the molecular orbitals of the tetrameric units of complexes **1** and **2**. The distribution of frontier orbitals was determined by using the sto-3g* basis set with the Gaussian 03 program at the workstation. The calculation continued until the root mean square (RMS) gradient was less than 0.188 kcal mol^{-1}.

Differential pulse voltammetry measurements: Differential pulse voltammetry studies were recorded with a CHI650 electrochemical analyzer utilizing the three-electrode configuration, composed of a Pt working electrode, a Pt auxiliary electrode, and a commercially available saturated calomel electrode as the reference electrode with a pure N_2 gas inlet and outlet. The measurements were performed in DMF containing tetrabutylammonium perchlorate (nBu$_4$NClO$_4$) (0.1 mol dm^{-3}) as supporting electrolyte, which has a 50 ms pulse width and a 20 ms sample width. The potential was scanned from +0.2 to +0.7 V at a scan rate of 20 mV s^{-1}.

Nonlinear optical measurements: A solution of **1**, **2**, or H_2FMPA in DMF was placed in a 1 mm quartz cuvette for NLO measurements. The nonlinear refraction was measured with a linearly polarized laser light (λ = 532 nm; pulse width = 7 ns) generated from a Q-switched and frequency-doubled Nd:YAG laser. The spatial profiles of the optical pulses were nearly Gaussian. The laser beam was focused with a 25 cm focal-length focusing mirror. The radius of the beam waist was measured to be 35 ± 5 μm (half-width at $1/e^2$ maximum). The interval between the laser pulses was chosen to be ≈5 s for operational convenience. The incident and transmitted pulse energies were measured simultaneously by two Laser Precision detectors (RjP-735 energy probes), which were linked to a computer by an IEEE interface. The NLO properties of the samples were manifested by moving the samples along the axis of the incident beam (Z direction) with respect to the focal point.[67] An aperture of 0.5 mm in radius was placed in front of the detector to assist the measurement of the self-focusing effect.

Structure determination: Crystal data and experimental details for complexes **1** and **2** are contained in Table S1 in the Supporting Information. Suitable single crystals with dimensions of 0.20× 0.18×0.18 mm for **1** and 0.20× 0.20×0.20 mm for **2** were selected for single-crystal X-ray diffraction analysis. Data collection was performed on a Rigaku RAXIS-IV image plate area detector for study using graphite-monochromated $Mo_{K\alpha}$ (λ = 0.71073 Å) radiation at 291(2) K by using the ω-2θ scan technique. The data were corrected for Lorentz and polarization factors and for absorption by using empirical scan data. The structure was solved with the SHELX program,[68] and refined by full-matrix least squares methods based on F^2,[69] with anisotropic thermal parameters for the non-hydrogen atoms. The hydrogen atoms were located theoretically and not refined. Selected bond lengths and bond angles are listed in Tables 1 and 2.

Table 1. Selected bond lengths [Å] and angles [°] for **1**.[a]

Cd1−O6	2.138(5)	Cd1−O3	2.208(4)
Cd1−O2#1	2.278(4)	Cd1−N1	2.305(5)
Cd1−N2	2.353(5)	Cd2−O4#1	2.151(5)
Cd2−O1#1	2.243(4)	Cd2−N4	2.339(5)
Cd2−O2	2.342(4)	Cd2−N3	2.352(4)
Cd2−O3	2.642(5)	Cd3−O11	2.148(5)
Cd3−O8#2	2.226(4)	Cd3−O9	2.250(5)
Cd3−N5	2.328(5)	Cd3−N6	2.343(5)
Cd4−O10	2.155(5)	Cd4−O7#2	2.212(4)
Cd4−N7	2.338(5)	Cd4−N8	2.351(5)
Cd4−O9	2.358(4)	N1-Cd1-N2	71.77(17)
O6-Cd1-O3	107.49(16)	O6-Cd1-O2#1	99.74(16)
O3-Cd1-O2#1	98.30(14)	O6-Cd1-N1	107.36(17)
O3-Cd1-N1	140.98(17)	O2#1-Cd1-N1	92.60(16)
O6-Cd1-N2	101.73(17)	O3-Cd1-N2	84.46(15)
O2#1-Cd1-N2	156.43(17)	N3-Cd2-O3	95.59(15)
O4#1-Cd2-O1#1	99.25(18)	O4#1-Cd2-N4	102.22(18)
O1#1-Cd2-N4	151.15(17)	O4#1-Cd2-O2	99.41(15)
O1#1-Cd2-O2	101.57(14)	N4-Cd2-O2	93.73(16)
O4#1-Cd2-N3	106.45(17)	O1#1-Cd2-N3	84.54(16)
N4-Cd2-N3	71.07(17)	O2-Cd2-N3	152.15(16)
O4#1-Cd2-O3	157.95(14)	O1#1-Cd2-O3	81.85(15)
N4-Cd2-O3	85.35(16)	O2-Cd2-O3	59.11(13)
Cd1-O3- Cd2	105.56(15)	O11-Cd3-O8#2	113.19(18)
O11-Cd3-O9	101.54(17)	O8#2-Cd3-O9	96.46(16)
O11-Cd3-N5	104.00(19)	O9-Cd3-N5	150.87(18)
O11-Cd3-N6	103.10(18)	O8#2-Cd3-N6	141.04(18)
O9-Cd3-N6	89.52(17)	N5-Cd3-N6	71.29(18)
O10-Cd4-O7#2	102.99(19)	O10-Cd4-N7	108.83(18)
O10-Cd4-N8	94.21(18)	N7-Cd4-N8	71.19(18)
O10-Cd4-O9	92.73(17)	O7#2-Cd4-O9	95.92(16)

[a] Symmetry transformations used to generate equivalent atoms: #1: $-x$, $-y$, $-z+1$; #2: $-x$, $-y$, $-z$.

Table 2. Selected bond lengths [Å] and angles [°] for **2**.[a]

Zn1−O5	1.949(6)	Zn1−O2#1	2.004(6)
Zn1−O1	2.099(5)	Zn1−N2	2.162(7)
Zn1−N1	2.168(7)	Zn2−O4	1.943(6)
Zn2−O3#1	2.021(5)	Zn2−O1	2.140(5)
Zn2−N4	2.174(7)	Zn2−N3	2.195(6)
Zn3−O7	1.915(5)	Zn3−O10	1.982(5)
Zn3−N6	2.122(7)	Zn3−O12#2	2.140(5)
Zn3−N5	2.222(6)	Zn4−O8	1.950(6)
Zn4−O11	2.007(5)	Zn4−N7	2.165(7)
Zn4−O12#2	2.165(5)	Zn4−N8	2.169(7)
O5-Zn1-O2#1	112.5(3)	O5-Zn1-O1	102.0(2)
O2#1-Zn1-O1	94.2(2)	O5-Zn1-N2	101.8(2)
O2#1-Zn1-N2	84.9(2)	O1-Zn1-N2	154.6(2)
O5-Zn1-N1	99.9(3)	O2#1-Zn1-N1	145.4(2)
O1-Zn1-N1	90.6(2)	N2-Zn1-N1	76.6(2)
O4-Zn2-O3#1	106.2(2)	O4-Zn2-O1	97.0(2)
O3#1-Zn2-O1	93.8(2)	O4-Zn2-N4	109.9(3)
O3#1-Zn2-N4	87.4(2)	O1-Zn2-N4	151.6(2)
O4-Zn2-N3	91.3(2)	O3#1-Zn2-N3	159.2(3)
O1-Zn2-N3	95.3(2)	N4-Zn2-N3	75.8(3)
O7-Zn3-O10	112.8(2)	O7-Zn3-N6	103.2(2)
O10-Zn3-N6	141.3(2)	O7-Zn3-O12#2	99.6(2)
O10-Zn3-O12#2	94.5(2)	N6-Zn3-O12#2	93.2(2)
O7-Zn3-N5	101.2(2)	O10-Zn3-N5	83.5(2)
N6-Zn3-N5	75.8(2)	O12#2-Zn3-N5	158.3(2)
O8-Zn4-O11	101.2(2)	O8-Zn4-N7	107.9(2)
O11-Zn4-N7	85.1(2)	O8-Zn4-O12#2	101.5(2)
O11-Zn4-O12#2	96.1(2)	N7-Zn4-O12#2	149.8(2)
O8-Zn4-N8	97.9(3)	O11-Zn4-N8	156.2(3)
N7-Zn4-N8	75.6(3)	O12#2-Zn4-N8	93.8(2)

[a] Symmetry transformations used to generate equivalent atoms: #1: $-x$, $-y$, $-z+1$; #2: $-x$, $-y$, $-z$.

CCDC-262564 and CCDC-262565 contain the supplementary crystallographic data for this paper. These data can be obtained free of charge from the Cambridge Crystallographic Data Centre via www.ccdc.cam.ac.uk/data_request/cif.

Acknowledgements

We thank the National Natural Science Foundation of China (Nos. 2001006 and 20371042) for support.

[1] A. Clearfield, *Prog. Inorg. Chem.* **1998**, *47*, 371–510.
[2] A. Clearfield, M. Casciola, U. Costantino, *Compr. Supermol. Chem.* **1996**, *7*, 107–149.
[3] G. Cao, H.-G. Hong, T. E. Mallouk, *Acc. Chem. Res.* **1992**, *25*, 420–427.
[4] J.-D. Wang, A. Clearfield, G.-Z. Peng, *Mater. Chem. Phys.* **1993**, *35*, 208–216.
[5] S. Cheng, G.-Z. Peng, A. Clearfield, *Ind. Eng. Chem. Prod. Res. DeV.* **1984**, *23*, 219–225.
[6] A. Clearfield, *Curr. Opin. Solid State Mater. Sci.* **1996**, *1*, 268–278.
[7] E. I. Tolis, M. Helliwell, S. Langley, J. Raftery, R. E. P. Winpenny, *Angew. Chem.* **2003**, *115*, 3934–3938; *Angew. Chem. Int. Ed.* **2003**, *42*, 3804–3808.
[8] Y. Yang, J. Pinkas, M. Noltemeyer, H.-G. Schmidt, H. W. Roesky, *Angew. Chem.* **1999**, *111*, 706–708; *Angew. Chem. Int. Ed.* **1999**, *38*, 664–666.
[9] C. Lei, J.-G. Mao, Y.-Q. Sun, H.-Y. Zeng, A. Clearfield, *Inorg. Chem.* **2003**, *42*, 6157–6159.
[10] V. Chandrasekhar, S. Kingsley, B. Rhatigan, M. K. Lam, A. L. Rheingold, *Inorg. Chem.* **2002**, *41*, 1030–1032.
[11] D.-K. Cao, Y.-Z. Li, L.-M. Zheng, *Inorg. Chem.* **2005**, *44*, 2984–2985.
[12] G. Anantharaman, V. Chandrasekhar, M. G. Walawalkar, H. W. Roesky, D. Vidovic, J. Magull, M. Noltemeyer, *Dalton Trans.* **2004**, 1271–1275.
[13] G. Anantharaman, M. G. Walawalkar, R. Murugavel, B. Gabor, R. Herbst-Irmer, M. Baldus, B. Angerstein, H. W. Roesky, *Angew. Chem.* **2003**, *115*, 4620–4623; *Angew. Chem. Int. Ed.* **2003**, *42*, 4482–4485.
[14] V. Chandrasekhar, S. Kingsley, *Angew. Chem.* **2000**, *112*, 2410–2412; *Angew. Chem. Int. Ed.* **2000**, *39*, 2320–2322.
[15] V. Chandrasekhar, L. Nagarajan, K. Gopal, V. Baskar, P. Koegerler, *Dalton Trans.* **2005**, 3143–3145.
[16] E. K. Brechin, R. A. Coxall, A. Parkin, S. Parsons, P. A. Tasker, R. E. P. Winpenny, *Angew. Chem.* **2001**, *113*, 2772–2775; *Angew. Chem. Int. Ed.* **2001**, *40*, 2700–2703.
[17] S. J. Langley, M. Helliwell, R. Sessoli, P. Rosa, W. Wernsdorfer, R. E. P. Winpenny, *Chem. Commun.* **2005**, 5029–5031.
[18] W. F. Ruettinger, G. C. Dismukes, *Inorg. Chem.* **2000**, *39*, 1021–1027.
[19] H.-C. Yao, Y.-Z. Li, Y. Song, Y.-S. Ma, L.-M. Zheng, X.-Q. Xin, *Inorg. Chem.* **2006**, *45*, 59–65.
[20] M. G. Walawalkar, R. Murugavel, A. Voigt, H. W. Roesky, H.-G. Schmidt, *J. Am. Chem. Soc.* **1997**, *119*, 4656–4661.
[21] V. Chandrasekhar, V. Baskar, A. Steiner, S. Zacchini, *Organometallics* **2002**, *21*, 4528–4532.
[22] M. I. Khan, J. Zubieta, *Prog. Inorg. Chem.* **1995**, *43*, 1–149, and references therein.
[23] Y.-P. Zhang, A. Clearfield, *Inorg. Chem.* **1992**, *31*, 2821–2826.
[24] C. Bellitto, E. M. Bauer, S. A. Ibrahim, M. R. Mahmoud, G. Righini, *Chem. Eur. J.* **2003**, *9*, 1324–1331.
[25] G. B. Hix, K. D. M. Harris, *J. Mater. Chem.* **1998**, *8*, 579–584.
[26] B.-L. Zhang, A. Clearfield, *J. Am. Chem. Soc.* **1997**, *119*, 2751–2752.
[27] C. V. K. Sharma, A. Clearfield, *J. Am. Chem. Soc.* **2000**, *122*, 1558–1559.

[28] H. L. Ngo, W.-B. Lin, *J. Am. Chem. Soc.* **2002**, *124*, 14298–14299.
[29] J.-G. Mao, Z. Wang, A. Clearfield, *J. Chem. Soc. Dalton Trans.* **2002**, 4541–4546.
[30] I. Lukes, J. Kotek, P. Vojtisek, P. Hermann, *Coord. Chem. Rev.* **2001**, *216–217*, 287–312.
[31] J. Kotek, P. Lubal, P. Hermann, I. Císaøová, I. Lukes, T. Godula, I. Svobodová, P. Táborský, J. Havel, *Chem. Eur. J.* **2003**, *9*, 233–248.
[32] E. M. Sabbar, M. E. D. Roy, J. P. Besse, *Mater. Res. Bull.* **2000**, *35*, 93–107.
[33] P. M. Di Giacomo, M. B. Dines, *Polyhedron* **1982**, *1*, 61–68.
[34] C.-Y. Yang, A. Clearfield, *React. Polym., Ion Exch., Sorbents* **1987**, *5*, 13–21.
[35] J.-L. Song, H.-H. Zhao, J.-G. Mao, K. R. Dunbar, *Chem. Mater.* **2004**, *16*, 1884–1889.
[36] S. J. Hartman, E. Todorov, C. Cruz, S. C. Sevov, *Chem. Commun.* **2000**, 1213–1214.
[37] J. Kotek, P. Lebdusková, P. Hermann, L. V. Elst, R. N. Muller, C. F. G. C. Geraldes, T. Maschmeyer, I. Lukes, J. A. Peters, *Chem. Eur. J.* **2003**, *9*, 5899–5915.
[38] O. Oms, J. L. Bideau, F. Leroux, A. Lee, D. Leclercq, A. Vioux, *J. Am. Chem. Soc.* **2004**, *126*, 12090–12096.
[39] W. Henderson, S. R. Alley, *Inorg. Chim. Acta* **2001**, *322*, 106–112.
[40] H.-W. Hou, G. Li, L.-K. Li, Y. Zhu, X.-R. Meng, Y.-T. Fan, *Inorg. Chem.* **2003**, *42*, 428–435.
[41] P. Bergamini, S. D. Martino, A. Maldotti, S. Sostero, *J. Organomet. Chem.* **1989**, *365*, 341–346.
[42] L. H. Ali, A. Cox, T. J. Kamp, *J. Chem. Soc. Dalton Trans.* **1973**, 1468–1474.
[43] G. B. Hix, B. M. Kariuki, S. Kitchin, M. Tremayne, *Inorg. Chem.* **2001**, *40*, 1477–1481.
[44] Harris notation describes the binding mode as $[X.Y_1Y_2Y_3\ldots Y_n]$, in which X is the overall number of metals bound by the whole ligand, and each value of Y refers the number of metal atoms attached to the different donor atoms. See: R. A. Coxall, S. G. Harris, D. K. Henderson, S. Parsons, P. A. Tasker, R. E. P. Winpenny, *J. Chem. Soc. Dalton Trans.* **2000**, 2349–2356.
[45] G. Yu, S.-W. Yin, Y.-Q. Liu, Z.-G. Shuai, D.-B. Zhu, *J. Am. Chem. Soc.* **2003**, *125*, 14816–14824.
[46] J.-H. Yang, S.-L. Zheng, X.-L. Yu, X.-M. Chen, *Cryst. Growth Des.* **2004**, *4*, 831–836.
[47] X.-R. Meng, H.-W. Hou, G. Li, B.-X. Ye, T.-Z. Ge, Y.-T. Fan, Y. Zhu, H. Sakiyama, *J. Organomet. Chem.* **2004**, *689*, 1218–1229.
[48] G. Li, H.-W. Hou, L.-K. Li, X.-R. Meng, Y.-T. Fan, Y. Zhu, *Inorg. Chem.* **2003**, *42*, 4995–5004.
[49] D. Guo, Y.-T. Li, C.-Y. Duan, H. Mo, Q.-J. Meng, *Inorg. Chem.* **2003**, *42*, 2519–2530.
[50] T. Mitsumori, M. Bendikov, O. Dautel, F. Wudl, T. Shioya, H. Sato, Y. Sato, *J. Am. Chem. Soc.* **2004**, *126*,16793–16803.
[51] B. J. Coe in *Comprehensive Coordination Chemistry II, Vol. 9* (Eds.: J. A. McCleverty, T. J. Meyer), Pergamon, Oxford, **2004**, pp. 621–687.
[52] J. C. Calabrese, L.-T. Cheng, J. C. Green, S. R. Marder, W. Tam, *J. Am. Chem. Soc.* **1991**, *113*, 7227–7232.
[53] Y. Liao, B. E. Eichinger, K. A. Firestone, M. Haller, J.-D. luo, W. Kaminsky, J. B. Benedict, P. J. Reid, A. K. Jen, L. R. Dalton, B. H. Robinson, *J. Am. Chem. Soc.* **2005**, *127*, 2758–2766.
[54] N. J. Long, *Angew. Chem.* **1995**, *107*, 37–56; *Angew. Chem. Int. Ed. Engl.* **1995**, *34*, 21–38.
[55] G. Li, Y.-L. Song, H.-W. Hou, L.-K. Li, Y.-T. Fan, Y. Zhu, X.-R. Meng, L.-W. Mi, *Inorg. Chem.* **2003**, *42*, 913–920.
[56] H. Chao, R.-H. Li, B.-H. Ye, H. Li, X.-L. Feng, J.-W. Cai, J.-Y. Zhou, L.-N. Ji, *J. Chem. Soc. Dalton Trans.* **1999**, 3711–3717.
[57] M. Sheik-Bahae, A. A. Said, T. H. Wei, D. J. Hagan, E. W. Van Stryland, *IEEE J. Quantum Electron.* **1990**, *26*, 760–769.
[58] S. Shi, Z. Lin, Y. Mo, X.-Q. Xin, *J. Phys. Chem.* **1996**, *100*, 10696–10700.
[59] W.-B. Lin, Z.-Y. Wang, L. Ma, *J. Am. Chem. Soc.* **1999**, *121*, 11249–11250.
[60] H.-W. Hou, X.-R. Meng, Y.-L. Song, Y.-T. Fan, Y. Zhu, H.-J. Lu, C.-X. Du, W.-H. Shao, *Inorg. Chem.* **2002**, *41*, 4068–4075.
[61] H.-W. Hou, Y.-L. Wei, Y.-L. Song, L.-W. Mi, M.-S. Tang, L.-K. Li, Y.-T. Fan, *Angew. Chem.* **2005**, *117*, 6221–6228; *Angew. Chem. Int. Ed.* **2005**, *44*, 6067–6074.
[62] Y.-S. Chen, Y.-X. Wang, S. Ye, *Int. J. Quantum Chem.* **2005**, *103*, 60–70.
[63] S. R. Alley, W. Henderson, *J. Organomet. Chem.* **2001**, *637–639*, 216–229.
[64] A. D. Becke, *Phys. ReV. A* **1988**, *38*, 3098–3100.
[65] A. D. Becke, *J. Chem. Phys.* **1993**, *98*, 5648–5652.
[66] C. Lee, W. Yang, R. G. Parr, *Phys. Rev. B* **1988**, *37*, 785–789.
[67] M. Sheik-Bahae, A. A. Said, E. W. Van Stryland, *Opt. Lett.* **1989**, *14*, 955–957.
[68] G. M. Sheldrick, SHELXS-97, Program for Crystal Structure Solution, University of Göttingen (Germany), **1997**.
[69] G. M. Sheldrick, SHELXL-97, Program for Crystal Structure Refinement, University of Göttingen (Germany), **1997**.

Received: July 28, 2005
Revised: March 11, 2006
Published online: May 24, 2006

